

Temperature influence on a linear array of coupled Sal'nikov oscillators: the muscle fiber scenario

Daniel Barragán & Pablo Ochoa-Botache

Universidad Nacional de Colombia, sede Medellín, Facultad de Ciencias, Medellín, Colombia. dabarraganra@unal.edu.co, paochoab@unal.edu.co

Received: March 1st, 2022. Received in revised form: October 12th, 2022. Accepted: November 10th, 2022.

Abstract

Muscles are thermogenic organs for adult mammals and birds but can also be thermosensitive. In this respect, recent research has shown the excitability of cardiac muscle tissue when irradiated with infrared laser light. Likewise, intrinsic muscle function should give place to local thermal gradients, either because of Ca^{2+} -ATPase thermoregulatory mechanisms or, specifically in the skeletal muscle, after intense exercise. Alongside internal thermal gradients, muscle fatigue characterizes by stressful cellular conditions. Similar to stress-like conditions has been documented in myocytes from rats, the emergence of oscillations of important biochemical species [1]. We show how a thermal gradient or a thermal pulse influences the dynamics of biochemical oscillations in a simplified biochemical model of muscle fiber and discuss the consequences in a living muscle. For this purpose, each simplified sarcomere behavior is governed according to a modified Sal'nikov model, as proposed in a previous paper [2].

Keywords: skeletal muscle; cardiomyocytes; contraction; heat pulses; Sal'nikov model; thermal gradient.

Influencia de la temperatura en un arreglo lineal de osciladores Sal'nikov acoplados: escenario en una fibra muscular

Resumen

Los músculos son órganos termogénicos en los mamíferos adultos y las aves, pero también pueden actuar como sistemas termosensibles. Por ejemplo, investigaciones recientes han mostrado la excitabilidad del tejido muscular cardíaco cuando se irradia con luz infrarroja. Del funcionamiento inherente del músculo aparecen gradientes térmicos, ya sea por mecanismos termorregulatorios de la Ca^{2+} -ATPasa o, en el músculo esquelético, después de ejercicio intenso. Junto con los gradientes térmicos, la fatiga muscular está caracterizada por condiciones celulares de estrés. Se ha documentado que en estas condiciones en los miocitos de rata aparecen oscilaciones de especies bioquímicas importantes [1]. Nosotros mostramos cómo un gradiente térmico, o un pulso térmico, influencia la dinámica de oscilaciones bioquímicas en un modelo simplificado de una fibra muscular y discutimos posibles consecuencias en el tejido vivo. Para este propósito, cada sarcómero se modela de acuerdo con el modelo Sal'nikov simplificado, como se propuso en un artículo anterior [2].

Palabras clave: músculo esquelético; cardiomiocito; contracción muscular; pulso de calor; modelo Sal'nikov; gradiente térmico.

1 Introduction

Muscles in adult mammals and birds are responsible for most heat generation to keep their organisms thermoregulated [3]. Nevertheless, it has recently been stated that they could also act as a thermosensitive system [4]. Experiments conducted over muscle fibers from cardiac tissue reveal that local thermal perturbation caused using infrared (IR) laser light influences the dynamic response of

the fibers. The thermal excitability of real striated myofibrils was addressed before isolating an acting chain and applying a heat pulse [5,6]. Although a skeletal muscle fiber is susceptible to displaying a similar response when stimulated with a spot laser IR, all efforts have been centered on cardiac cells. One example is the increasing number of studies showing how applying laser light pulses makes it possible to pace from groups of cardiomyocytes to an embryonic heart [4,7,8]. Besides muscle systems, local thermal gradients have

How to cite: Barragán, D. and Ochoa-Botache, P., Temperature influence on a linear array of coupled Sal'nikov oscillators: the muscle fiber scenario. DYNA, 89(224), pp. 99-106, October - December, 2022.

been recognized to affect intracellular behavior and alter physiological functions [9].

Two explanations to address the thermal influence in cardiomyocytes have been proposed. The first one treats the excitation-contraction process from a global perspective and suggests that the temperature gradient affects ion channel openings; this process is related to Ca^{2+} releasing from the sarcoplasmic reticulum. Rabbitt's group experiments [10] for photothermal excitation evince transient capacitive currents in a neuromuscular junction. Therefore, we should consider the interplays between myosin, tropomyosin, and actin instead of focusing on single cardiomyocytes or diverting attention away from the sarcomere. In this respect, Ishiwata's group found cardiomyocyte contractions without Ca^{2+} . They adduced contractions to a partial dissociation of tropomyosin from F-actin induced by heating, a self-reliant process from Ca^{2+} concentration [4]. Additionally, to the mechanism involved in the photothermal contractions, it seems that contractions depend strongly on the magnitude of the temperature increase (ΔT) as well as the variation of the temperature during the pulse application [4,10].

Until now, cardiac tissue has been excited externally using a laser light pulse that punctually heats the water, generating a thermal gradient in its surroundings. Furthermore, one of the primary purposes is to refine this tool to study living muscle tissue with minimum interference, something challenging to achieve through electrical stimulation; or even thinking of possible therapeutic applications. However, considering a muscle fiber, this thermal gradient also could be internally produced by the Ca^{2+} -ATPase sarcoplasmic reticulum, knowing that this pump, under some circumstances, does not follow a strict cycle [11,12]. When this happens, a 'slippage' or skip of the regular steps is observed, traduced in consuming ATP to produce heat, a thermogenic mechanism. In other contexts, for example, under skeletal muscle fatigue, such thermal gradient could be provided by the same intense muscle use.

When working out the skeletal muscle until fatigue, cellular metabolism is under stress, and preserving the energy state becomes a priority to the system [13]. In similar stress-like conditions, Yang et al. [1] have shown that myocytes from rat exhibit glycolytic oscillations and ATP oscillations. Thus, energy-supplying processes can display oscillatory behavior until physiological conditions are favorable again, which, although not confirmed experimentally, could be the case for a skeletal muscle fiber. Considering the internal thermal gradients generated as a consequence of muscle fatigue [14] or thermogenic process, they can be matched advantageously with biochemical oscillations to drive chemical energy production in the muscle tissue at the cellular level.

As presented above, coupling a thermal gradient with glycolytic oscillations is not an unlikely biochemical scenario. Theoretically, all that is needed is a model reaction capable of producing thermal and chemical oscillations. A Sal'nikov-modified model, including a third autocatalytic reaction, fulfills this requirement [2]. In that case, shifting from chemical oscillations (using autocatalytic reaction) to mixed thermal-chemical oscillations is possible.

Furthermore, if this model takes place in each functional

unit of a single fiber, i.e., each sarcomere, coupling several Sal'nikov-modified reactors will be equivalent to a single fiber. Each sarcomere is treated as a black box, sensitive to biochemical species and temperature changes. We are not scaling the model to reproduce the exact physical realization in a microscopic fiber scale because the main interest is the formulation of the governing equations to understand the interplay between thermal gradients and biochemical oscillations. With this restriction, we showed that several Sal'nikov-modified units (reactors) coupled through heat exchange let thermal gradients develop within a 1-dimensional macro sarcomere array (an ideal macroscopic analog of a muscle fiber). Moreover, the resulting fiber model is thermally perturbed, and its behavior is analyzed in the biochemical context of a skeletal muscle contraction.

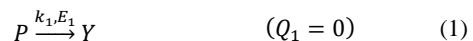
2 Materials and methods

2.1 Modified model Sal'nikov for chemical energy supplied to a muscle sarcomere

From a macroscopic scale, a striated muscle is formed by muscle fibers composed of myofibrils. Zooming a single myofibril reveals that each consists of cylindrical units called sarcomeres [15]. Sarcomeres are the largest ordered multi-protein assemblies; their most remarkable components are thick and thin filaments interlaced, nearly identical in length [16]. The thin filament comprises actin, troponin, tropomyosin, and myosin II motors from the thick filament at this microscopic scale. Each myosin molecule has two cross bridges that attach cyclically to the actin filament and move the actin along the myosin filament. As both filaments overlap, the sarcomere length gradually decreases. The visible result of summing the contribution of all sarcomeres will be the development of macroscopic force and muscle shortening [17,18]. The hydrolysis of ATP provides the energy required to complete the attaching-detaching cycle to ADP and Pi occurring at the myosin catalytic domain. The chemical reaction is coupled to a mechanical response [19].

Sal'nikov's modified model does not pretend to describe sarcomere at these scales. Instead, it focuses on the biochemical aspect of energetics requirement to make muscle contraction possible. In this sense, a sarcomere is comparable to a chemical reactor where a reaction occurs through ATP supply (macro-sarcomere), and the supply rate constrains the reaction time course. In fact, at the molecular level, the myosin cross-bridge is the transducer that interconverts chemical energy (derived from ATP) to mechanical work [20]. Thus, the proposed model intends to understand how thermal gradients can couple to biochemical oscillations of energetic species relevant to muscle function, i.e., ATP, rather than explain details of the sarcomere mechanism.

Sal'nikov's modified model proposed before [2] was based upon three differential equations (eq. 1-3), including two chemical (Y and Z) species and heat conduction. A parameter γ controls transition from pure thermal instabilities ($\gamma = 0$) to mixed thermal-chemical instabilities ($\gamma = 1$).





In this case, thermal dependence is linked to the conversion $Z \xrightarrow{k_3} B$ (the exothermic reaction with enthalpy $Q_3 \neq 0$), where k_3 takes the form of eq. (4):

$$k_3(T) = k_3(T_a) \exp(E_3/R \times \nabla T) \quad (4)$$

and $\nabla T = 1/T_a - 1/T$. Table 1 summarizes the parameter values used to simulate system dynamics according to eq. (1)-(4). In the set of governing differential equations, V is the reactor volume, C_p , the heat capacity of the mixture, S is the reactor surface area, χ is the surface heat transfer coefficient and T_a , the surrounding temperature. The concentration of each chemical specie is presented in lower caps. Heat loss is modeled as a simple Newtonian heat transfer, assuming a well-stirred solution.:

$$\frac{dy}{dt} = p_0 k_1 \exp(-k_1 t) - k_2 y \quad (5)$$

$$\frac{dz}{dt} = k_2 y - k_3 z^\gamma \quad (6)$$

$$\frac{dT}{dt} = \frac{1}{nC_p} [VQ_3 k_3 z - S\chi(T - T_a)] \quad (7)$$

To couple several of Sal'nikov's modified systems, the actual model is discretized using the finite differences method. Then eq. (5)-(7) will look like an equation set defined by eq. (8)-(10), keeping in mind that the value for γ is set to $\gamma = 1$ along the paper. When rewritten, the differential equations are set, and the term $p_0 k_1 \exp(-k_1 t)$ was assumed constant under chemical pool approximation for P specie and denoted v_p . Denoting by i the spatial step associated with a discrete compartment and by super index j a time step, then:

$$y_i^j = y_i^{j-1} + \Delta t [v_p - k_2 y_i^j] \quad (8)$$

$$z_i^j = z_i^{j-1} + \Delta t [k_2 y_i^j - k_3 z_i^j] \quad (9)$$

$$T_i^j = T_i^{j-1} + \frac{\Delta t}{nC_p} \left[VQ_3 k_3 z_i^j - S\chi(T_i^j - T_a) + \frac{\kappa_{trans}}{(\Delta x)^2} (T_{i+1}^j - 2T_i^j + T_{i-1}^j) \right] \quad (10)$$

Here, κ_{trans} represents the heat transfer coefficient between two adjacent compartments. Note that coupling was made only in Fourier's heat transfer law, and there is no chemical exchange. Doing $\kappa_{trans} = 0$, in eq. (10), reduces it to eq. (7). It makes sense when thinking about the selectivity of a cell membrane.

2.2 Configuration entropy tool to characterize the system

As mentioned, the present study aims to model chemical energy supply over time to a macro sarcomere unit. After bringing together enough sarcomeres, a myofibril is confirmed. As a result, the chemical energy input of myofibrils is a series of eq. (8)-(10) takes place. A sample of 400 compartments was arranged in a 1-dimensional linear array, and the initial thermal gradient (slope of the linear gradient, m), thermal pulse applying-time (t_{app}) as well as pulse amplitude (T_Δ) were varied to construct a phase diagram (see variables tested in Table 2). The compartment's initial temperature T_i , where i -th is defined according to the equation of a straight line $T_i = m \cdot i + T_{max}$, where $T_{max} = 300$ K and the slope m varies between 0.01 and 0.1 K/ i -th compartments (Fig. 2). Pulses were applied each 5 s, starting from 40 s to 70 s and affected only the first half of the compartments ($i = 0$ to $i = 200$). A typical 2D contour plot, like that in Figure 1, is drawn when running simulations with the combinations of variables previously described and summarized in Table 2. (Fig. 1 shows the evolution of the 1-dimensional array on the "Compartment" axis projected in the temporal axis and the "Temperature" axis).

Naturally, covering different initial thermal conditions and applying thermal pulses of different intensities or at other times will be reflected in an extensive collection of plots. Each 2D natural contour plot is resized to obtain helpful information from those pictures until receiving sides of the same length L . Thus, raw images are reduced to 5000×5000 pixels and displayed in black and white mode, associating each black pixel with one and a white pixel with a 0. This way, the same image is interpreted as a matrix filled with zeroes or ones. All this pre-processing stage prepares a particular image to be analyzed through configuration entropy as described by Andraud et al. [21,22]. The 2D contour plots generated from each simulation by employing configuration entropy are treated as disordered morphologies and characterized with a descriptor that describes their fractal structure [23]. This method has been used to describe fractal landscapes to clay soil samples and even fat, connective tissue [23–25]. This analysis method qualitatively describes the 1-dimensional array response to different conditions. It provides information about the system's behavior only under the restrictions imposed. An analytical stability analysis from eq could achieve a more general analysis. (8)-(10).

Table 1.

Representative values of Sal'nikov's physicochemical quantities.

| Physicochemical quantity | Symbol | Value |
|-----------------------------------|--|--|
| Volume | V | 1.0 dm ³ (cylindrical reactor with height $h = 0.15$ m and $r = 0.046$ m) |
| Surface area | S | Five dm ² |
| Surrounding temperature | T_a | 400 K |
| Activation energy | E_2 or E_3 | 166 kJ mol ⁻¹ |
| Heat capacity | C_p | 0.029 kJ K ⁻¹ mol ⁻¹ |
| Surface heat transfer coefficient | χ | 0.055 kJ s ⁻¹ dm ⁻² K ⁻¹ |
| Enthalpy of exothermic step | Q_3 | 400 kJ mol ⁻¹ |
| Initial reactant concentration | p_0 | Three $\times 10^{-3}$ mol dm ⁻³ |
| Rate constants | k_1 , k_2 and $k_{3,0}$ take values as indicated on the figure's caption | |
| Gas constant | 0.008314 | 0.008314 kJ mol ⁻¹ K ⁻¹ |

Source: Adapted from Barragán and Ochoa-Botache, 2018.

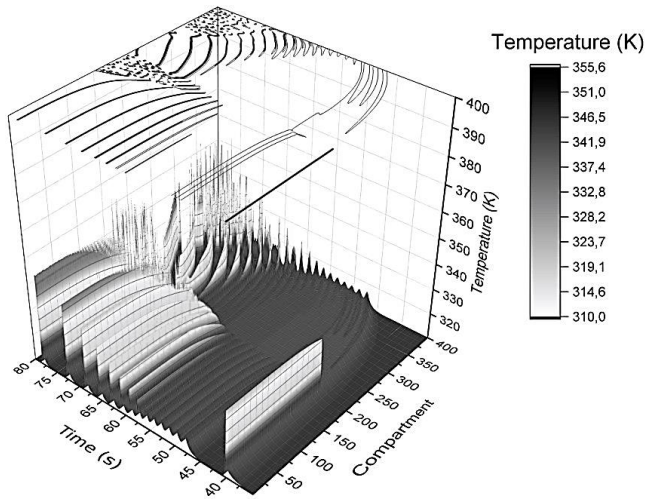


Figure 1. 3D profile showing the system's time evolution when a thermal pulse of amplitude 323.9 K was applied at $t_{app} = 40$ s, and the slope of the initial linear gradient was 0.1 K/ i -th compartment. At the top of the box is sketched the corresponding 2D contour plot, which will be the starting point for configuration entropy analysis. The X-axis corresponds to the i -th compartment (from compartment $i = 0$ to $i = 400$), the y-axis corresponds to the time, and the z-axis is the temperature (the gray color scale facilitates the interpretation of the contour plot). Source: Own elaboration.

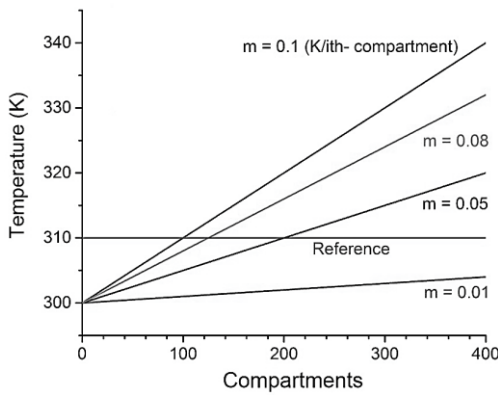


Figure 2. Thermal initial conditions imposed at time zero to each compartment, defined by the value of the slope m of a straight line. Reference temperature (green horizontal line, 310 K) is determined as the minimum temperature reached by the system in the frame of interest (40 – 80 s). Source: Own elaboration.

Table 2.

Set of conditions evaluated to construct a phase diagram of the system after being perturbed by a thermal pulse. Pulse was applied only to the first half of the compartments.

| Pulse applying time t_{app} (s) | Slope of the thermal gradient m (K/ i -th compartment) | Pulse amplitude T_{Δ} (K) |
|---|---|--|
| 40 | | |
| 45 | | |
| 50 | 0.01 | 317 |
| 55 | 0.05 | 320 |
| 60 | 0.08 | 323.9 |
| 65 | 0.10 | |
| 70 | | |

Source: Own elaboration

The prepared image is analyzed through a sliding square cell of side l . For a particular position of the cell, the number of pixels with value one contained in the cell is counted. Once the whole image is examined, it is computed $N_k(l)$, the number of cells containing k active pixels, and $N(l)$, the total number of visited cells. The probability associated with the state of the cell is thus defined as $p_k(l) = N_k(l)/N(l)$ and the corresponding entropy is:

$$H(l) = - \sum_{k=0}^{l^2} p_k(l) \log p_k(l) \quad (11)$$

which measures the uncertainty associated with the set of possible states the cell of size l may attain. $H(l)$ is an effective descriptor of the likelihood of the random pixel distribution which may occur inside a cell of size l . It is noteworthy that l cannot approach the size of the lattice since $p_k(l)$ would lose any real meaning, thus the condition $l < L/4$ is fixed. To examine the image structure at different length scales, the cell size is progressively increased. In accordance with those increments, entropy $H(l)$ changes, being necessary normalize its value in order to compare entropy values corresponding to different cell sizes. Then, for each l value the normalized entropy $H^*(l) = H(l)/H_{max}(l)$ is computed, where $H_{max}(l) = \log(l^2 + 1)$. $H^*(l)$ is called the configuration entropy of 2-dimensional morphology of the image [21–23]. Fig. 3 presents the configuration entropy analysis obtained from successive 2D contour plots where slope of the initial thermal gradient is 0.1 K/ i -th compartment and pulse amplitude is $T_{\Delta} = 323.9$ K. Value for configuration entropy allows distinguishing clearly when pulse is applied at $t_{app} = 40$ s (Fig. 4a, $H^* = 0.4095$) and $t_{app} = 70$ s (Fig. 4b, $H^* = 0.2746$). Qualitatively, the resulting image with more black pixels is associated with a higher H^* number (Fig. 4a has more black pixels than Fig. 4b). Fig. 5 summarizes the configuration entropy values obtained in the space of the parameters presented in Table 2.

3 Results and discussion

3.1 Overall effect of a thermal pulse

In these conditions, oscillatory chemical specie Z could be identified as ATP in a real fiber when restoring chemical energy is prioritized. Set of eq. (8)-(10) provides a compartmentalized energy supply model under such stressful conditions. A characteristic course time of temperature developed in a single 1-dimensional array is presented in Fig. 6. Fig. 8(d-f) presents the oscillatory transient in Z specie, which naturally is coupled to the thermal profile.

At this point, asking for the other compartments that complete the ideal muscle fiber outlook becomes logical. Each of them could be characterized with a plot of temperature vs. time or chemical concentration vs. time. However, the image obtained from the 3D plot of the fiber's time history is processed by the constitutive entropy method (a typical 2D contour plot shown in Fig. 1) instead of providing the evolutionary information of the system separately in this way. As a result, each image is numbered

from 0 to 1. The advantage of the configuration entropy tool lies in the possibility of discriminating with quantitative criteria an extensive collection of plots. This information is summarized in three 2D phase diagram plots generated after the maximum peak amplitude was set to 317, 320, and 323.9 K (Fig. 5). It can be seen that the zone, with the highest entropy value, is restricted to pulse applying time ranging from $t_{app} = 40$ s to 45 s. In the other coordinate, it is contained between $m = 0.08$ and $m = 0.1$ K/*i*-compartment.

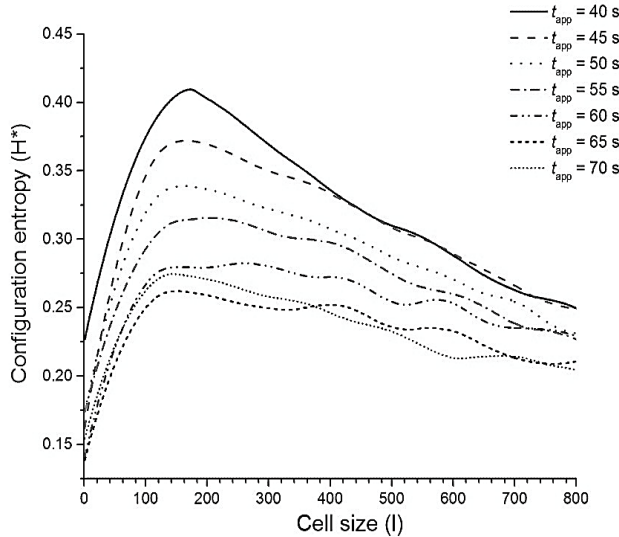


Figure 3. Configuration entropy was obtained after applying thermal pulses at different times. Configuration entropy (H^*) vs. analysis block size (l) of a 2D contour plot when T_{Δ} is fixed to 323.9 K and the slope of the initial linear gradient is 0.1 K/*i*-th compartments. H^* value is calculated from the maximum of each curve. Source: Own elaboration.

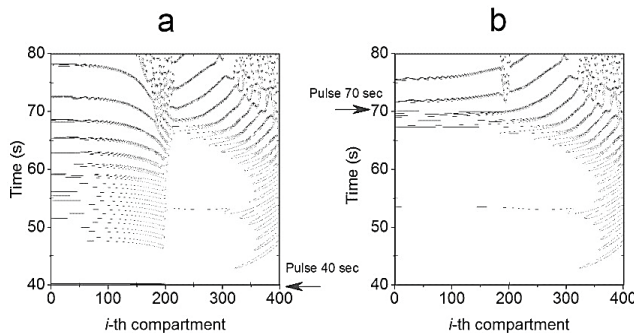


Figure 4. 2D thermal contour plot generated after the Pulse perturbed the system at (a) 40 s ($H^* = 0.4095$) and (b) 70 s ($H^* = 0.2746$), respectively. Source: Own elaboration.

Detailed configuration entropy values are reported in Fig. 7 and 8 when pulse amplitude was fixed to 317 (Fig. 7) and 323.9 K (Fig. 8). Again, the highest bars are contained in the region described above. This zone qualitatively implies a disordered morphological 2D structure associated with ordered structures. As the emergence of black pixels is tied to the number of oscillations exhibited in time, the zone with the highest entropy of Fig. 5 exhibits more oscillations (see

2D plot in Fig. 4a, where the pulse was applied for 40 s and has a higher $H_{40}^* = 0.4095$) than other regions (2D plot in Fig. 4b, where the pulse was applied at 70 s, with lower $H_{70}^* = 0.2746$).

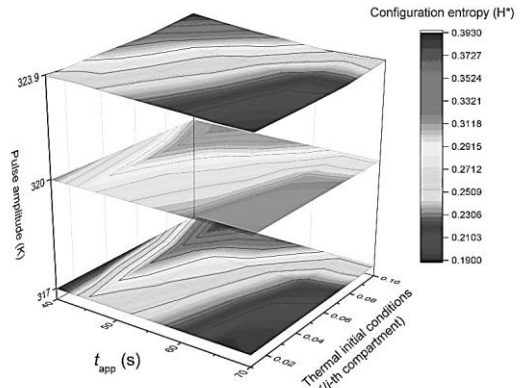


Figure 5. Summary of the results obtained using the configuration entropy analysis for different pulse amplitudes. Phase diagram collection summarizing the system's response after being thermally stimulated. Each plane corresponds to a different pulse amplitude response while varying on each of them the pulse-applying time t_{app} , and the slope m of initial thermal conditions (x-axis and y-axis). Source: Own elaboration.

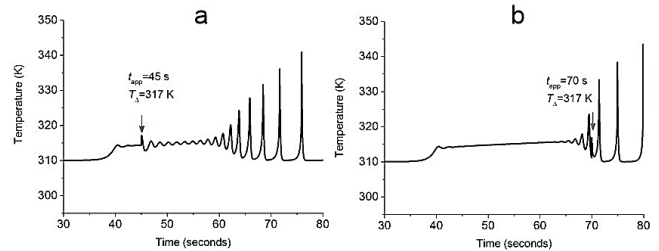


Figure 6. Time course of the first compartment's temperature for the plane at $T_{\Delta} = 317$ K related to (a) high and (b) low configuration entropy zones. In (a) pulse is applied at 45 s, and in (b) pulse is applied at 70 s. The slope of the linear gradient was 0.1 K/*i*-th compartment and 0.01 K/*i*-th compartment, respectively. Source: Own elaboration.

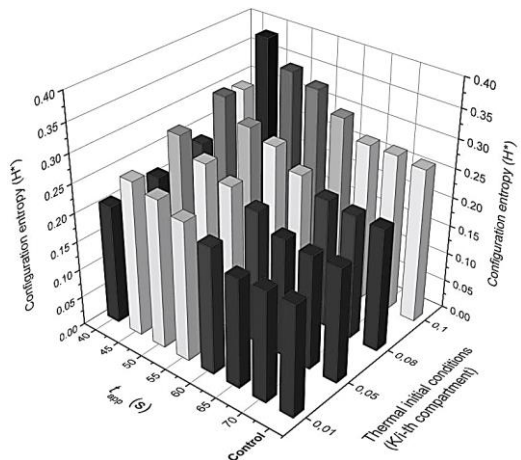


Figure 7. Detailed configuration entropy values reached by the system after being stimulated thermally by a pulse of 317 K. Source: Own elaboration.

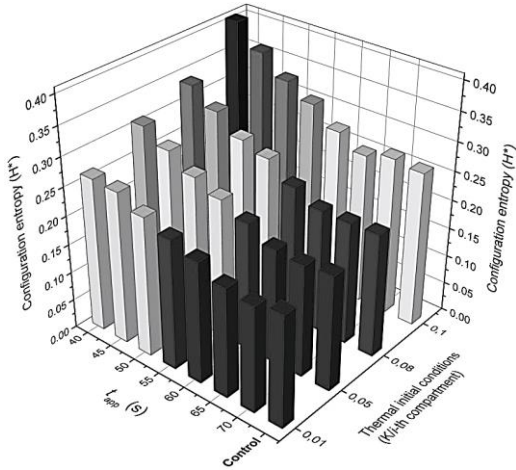


Figure 8. Detailed configuration entropy values reached by the system after being stimulated thermally by a pulse of 323.9 K. Pulse applying time and the slope of the thermal linear gradient were varied successively according to values reported in Table 2. Figures 6 and 7 are a 3D representation of the same 2D phase diagram presented in Fig. 3a. Source: Own elaboration.

In quantitative terms, if the thermal Pulse is applied before inherent oscillations start, the system responds with an oscillatory train (this is the case of Fig. 9(a-b)). The number of changes is proportional to the configuration entropy value in the time-compartments space, as shown in Fig. 3-4. However, if perturbation has no effect at the time of application of the Pulse, its amplitude is not comparable with the system's maximum amplitude. Correspondingly, the vibration of Fig. 9c applied at $t_{app} = 70$ s falls in a valley, making its relative amplitude not identical with the adjacent thermal spikes. Therefore, it does not significantly change the shape of the single-compartment temperature histories and the 2D contour plots are almost unchanged (see Fig. 7-8. Pulse and control applied at 70 s, i.e., Unperturbed systems exhibit similar entropy values). Therefore, it does not significantly change the shape of the single-compartment temperature histories, and the 2D contour plots are almost unchanged (see Figs. 7-8. Pulse and control applied at 70 s, i.e., Unperturbed systems exhibit similar entropy values). Instead, changes disappear once the Pulse is applied (figure not shown).

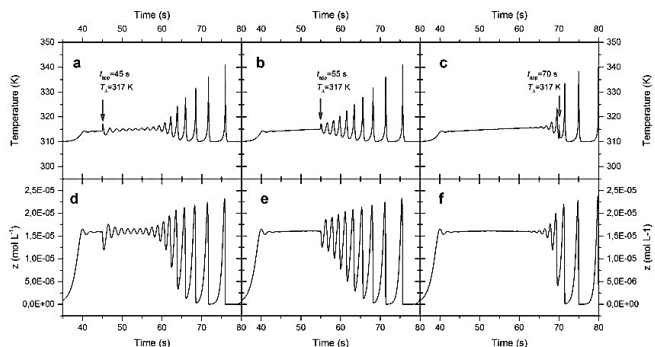


Figure 9. 2D graphs providing an overview of a single compartment ($i = 1$) response after being stimulated thermally. Each graph corresponds to a different thermal (a-c) or chemical (d-f) response. The slope of the initial thermal gradient was 0.1 K/ i -th compartment, and pulses of $T_{\Delta} = 317$ K were applied at times t_{app} 45, 55, and 70 s. Source: Own elaboration.

Besides the aspects concerning the pulse amplitude and when the system is perturbed, initial thermal conditions tend to increase configuration entropy. Linear thermal gradient slope, m , notoriously affects the behavior of the final half of the fiber, and even in the absence of perturbation, thermal spikes appear. A comparison between 2D contour plots from Fig. 4a and Fig. 4b hints that the upper part of both plots is the same, independent of the Pulse. In this sense, initial thermal conditions are absorbed like a thermal pulse. According to Fig. 2, at time $t = 0$, the last compartment should start with a temperature between 320 – 340 K if m is picked from $m = 0.05$ to $m = 0.1$ K/ i -th chamber. However, when $m = 0.1$ K/ i -th compartment, the last room is not heated until the reference value of 310 K. Precisely, for the latter, Figs. 7-8 reports the minimum configuration entropy values concerning other possible initial conditions.

3.2 Discussion

When a muscle fiber is exhausted after high exercise loads, depletion of ATP is expected near the Ca^{2+} -ATPases [26]. Oxidative metabolism or pools of energetically representative chemical species like PCr cannot maintain a continuous ATP feed at high rates and will be exhausted sooner or later. This ATP is essential to keep the Ca^{2+} ions exchange, which plays a fundamental role in the attaching-detaching cycle of myosin-actin filaments. At first sight, an ATP deficit at this level implies stopping all the machinery related to muscle movement. Nevertheless, being quiet is not as bad since an additional chemical impulse could lead to irreversible damage to the tissue [27]. The inconvenience would not be the ceasing of machinery's activity. Still, the time it takes to recover could be reduced if ATP is restored, and not precisely by the oxidative metabolism pathway.

These ideas were developed in a previous paper [2], where a chemical energy inlet was modeled for a single sarcomere. In such cases, it showed the relevance of chemical oscillations coupled with the local thermal gradient in stressing conditions to replenish levels of a chemical species of interest, i.e., ATP. The set of equations proposed was based on a modified Sal'nikov model and summarized in the eq. (1)-(3). Through numerical analysis, parameters presented in Table 1 were found to reproduce chemical oscillatory behavior in the presence of thermal instabilities, i.e., doing $\gamma = 1$. This condition was the starting point for the present work since the main goal was to evaluate a thermal gradient synergistic effect. Either in the form of a heat pulse, as proposed by [4], or a thermal gradient arising from intense muscular work alongside a muscle fiber, non-isothermal conditions modify system dynamics. They could be an emergency mechanism to overwhelm muscle fatigue locally.

Under energetic stressing conditions [1,28], myocytes from rat exhibit glycolytic and sustained ATP oscillations. If, as proposed in the set of eq. (1)-(3), These oscillations are gradually introduced in γ in autocatalysis along an oscillating thermal gradient. A chemical and thermal explosion is observed when the $\gamma = 1$ state is reached. It is the portrait of a single reactor unit.

Thus, a single reactor is an oversimplified system hosting some reactions inside a sarcomere with enough detail to

capture the relation between the chemical species that promote oscillatory behaviors. A coupling of several identical reactors, connected through heat exchange only, will lead to the idea of a myofibril chemical energy supplier. In other words, the model of eq. (8)-(10) fuels each i -th sarcomere with an inlet of chemical specie Z , associated with ATP. This scenario requires the definition of a finite volume for the reactor to connect several units that resemble a macro myofibril. Still, this parameter is kept constant since the interest is centered on the reactions.

Additionally, the 1-dimensional array of reactors (ideal myofibril) is sensitive to thermal changes. Experimentally, the effect of thermal dependence on muscle function is studied with localized thermal stimulus over muscle tissue or single cells (c.f. [7,29,30]) rather than using single myofibrils. This limitation centers the discussion on the qualitative results shown here rather than a numerical comparison against available data.

The way the compartmentalized model distributes chemical energy when no thermal pulse or initial thermal gradient is present is precisely a near identical repetition of the Z profile and thermal profile from the first cell $i = 1$ to $i = 400$. This ideal case does not show an appreciable change between cells in time despite including thermal exchange from each compartment I with their surrounds. However, when initial thermal conditions of the compartments are forced to behave linearly, following the equation of a straight line, different slopes m reveal a notorious change, especially near the last portion of the compartments. This difference when changing initial thermal conditions is a consequence of Fourier's heat transfer coupling because this law forces two adjacent rooms to exchange heat at the fastest rate possible [5], and being this process slower or more evident between compartments with different temperatures $i = 0$ and $i = 400$.

The system is more perturbed with the highest value for m (see Fig. 2). In effect, Fig. 4a shows that, even when a thermal pulse is applied, if $m = 0.1$ K/ i -compartment, the last compartments respond with thermal spikes and, conversely, chemical spikes in Z (Fig. 9(a-d)). In general, phase diagrams from Fig. 5 confirm that this value of m is obtained as the highest value for configuration entropy. Even a system unperturbed by a heat pulse has a minimum configuration entropy associated if a thermal profile is imposed since the beginning. Alternatively, in other words, chemical and thermal oscillations arise only as a consequence of the linear initial thermal conditions for each compartment. For this reason, the height of the bars for the undisturbed (control) system in Fig. 7-8 is comparable with bars obtained after a pulse is applied for 70 s (where the Pulse has no visible effect).

Nevertheless, suppose a homogenous thermal gradient would be sufficient to activate all the compartments, i.e., to increase the amount of Z with the thermal burst. In that case, it is more likely that a natural fiber is under a non-homogenous thermal gradient. The linear gradient proposed here is only an ideal case, illustrating how the compartments 'feel' the thermal burst at different times. First compartments are the first affected by thermal explosions, and to the extent we move away to the last boxes, shots are delayed. For this

reason, the time course of temperature corresponding to the first compartments seems to be shifted in time concerning the last rooms. Besides, it implies that the chemical supplier model oscillates in time, but the temperature and, conversely, the concentration of Z , varies among compartments at a given time.

In addition to an initial thermal linear gradient, the system is perturbed with a heat pulse, and the observed response varies in function of Pulse applying time and pulse amplitude. Pulse affected only half of the cells, i.e., two hundred compartments. Pulse applying time is a critical parameter if the pulse amplitude is not higher than the maximum amplitude of the oscillation when it is applied. Therefore, between 40 s and 60 s, a pulse starting at 317 K has a significant impact in terms of configuration entropy because, in this range, the amplitude of the Pulse is greater than the temperature of the system (~ 315 K) (see Fig. 9(a-b)), promoting an oscillatory behavior just as the Pulse is applied. Something similar occurs with initial thermal conditions since for $m=0.5$ to $m=0.1$ K/ i -compartment, the initial temperature is over the reference temperature of the system, 310 K (see Fig. 2).

Contrary to non-homogenous initial thermal conditions, a thermal pulse impacts homogenous thermal initial conditions similarly. That means synchronizing the fiber's chemical energy production simultaneously and among thermally stimulated compartments. This thermal synchronization has been recognized as a valuable tool, for example, to pace embryonic hearts [7].

4 Conclusion

The thermal excitability of muscle tissue is essential for monitoring the thermoregulatory function and highlighting the thermosensitive function throughout the body. Under fatigue conditions, where there is an ATP deficit, restoring ATP levels could be a good coupling between a biochemical reaction, i.e., glycolysis, and a thermal gradient. Glycolytic oscillations have been reported under stressing energetic conditions, and thermal gradients can be induced externally.

The 1-D ideal fiber governed by Sal'nikov's modified model shows a chemical-thermokinetic coupling. Their response to different scenarios can be studied by varying three parameters (see Table 2): The slope of the initial thermal gradient (comparable to the internal angle developed naturally in a muscle fiber as a result of intense mechanical work); thermal Pulse applying time (external thermal stimulation to the thread); and pulse amplitude. Numerical simulations deliver a collection of 2D plots by combining these parameters. To understand the information quantitatively, we introduce a configuration entropy analysis where a 2D plot is associated with a single H^* number, between 0 and 1. 0 means a homogeneous image (no black pixels, no thermal oscillations) and a highly heterogeneous image (black pixels due to thermal oscillations). The initial thermal conditions following a linear profile along the fiber lead to thermal and chemical oscillations (according to the natural coupling implicit in the Sal'nikov modified model for each compartment). Moreover, applying a thermal pulse could develop further chemical changes in the Z species

associated with ATP, which could be a workaround to sustain muscle energetics in stressful conditions during short periods.

References

- [1] Yang, J.-H., Yang, L., Qu, Z. and Weiss, J.N., Glycolytic Oscillations in isolated rabbit ventricular myocytes. *Journal of Biological Chemistry*, 283(52), pp. 36321-36327, 2008. DOI: <https://doi.org/10.1074/jbc.M804794200>.
- [2] Barragán, D., Ochoa-Botache, P.A., Transition from thermokinetic to chemical instabilities in a modified Sal'nikov model. *Journal of the Brazilian Chemical Society*, 29, pp. 1406-1416, 2018. DOI: <https://doi.org/10.21577/0103-5053.20180003>.
- [3] Rowland, L.A., Bal, N.C. and Periasamy, M., The role of skeletal-muscle-based thermogenic mechanisms in vertebrate endothermy: Non-shivering thermogenic mechanisms in evolution. *Biological Reviews*, 90(4), pp. 1279-1297, 2015. DOI: <https://doi.org/10.1111/brv.12157>.
- [4] Oyama, K., Mizuno, A., Shintani, S.A., Itoh, H., Serizawa, T., Fukuda, N., Suzuki, M. and Ishiwata, S., Microscopic heat pulses induce contraction of cardiomyocytes without calcium transients. *Biochemical and Biophysical Research Communications*, 417(1), pp. 607-612, 2012. DOI: <https://doi.org/10.1016/j.bbrc.2011.12.015>.
- [5] Kawaguchi, T., Honda, H., Hatori, K., Imai, E. and Matsuno, K., Fourier's law of heat transfer and its implication to cell motility. *Biosystems*, 81(1), pp. 19-24, 2005. DOI: <https://doi.org/10.1016/j.biosystems.2005.01.003>.
- [6] Kawaguchi, T. and Honda, H., Unidirectional movement of an actin filament taking advantage of temperature gradients. *Biosystems*, 90(1), pp. 253-262, 2007. DOI: <https://doi.org/10.1016/j.biosystems.2006.08.008>.
- [7] Jenkins, M.W., Duke, A.R., Gu, S., Doughman, Y., Chiel, H.J., Fujioka, H., Watanabe, M., Jansen, E.D. and Rollins, A.M., Optical pacing of the embryonic heart. *Nature Photonics*, 4(9), pp. 623-626, 2010. DOI: <https://doi.org/10.1038/nphoton.2010.166>.
- [8] Smith, N.I., Kumamoto, Y., Iwanaga, S., Ando, J., Fujita, K. and Kawata, S., A femtosecond laser pacemaker for heart muscle cells. *Optics Express*, 16(12), pp. 8604-8616, 2008. DOI: <https://doi.org/10.1364/OE.16.008604>.
- [9] Sonna, L.A., Fujita, J., Gaffin, S.L. and Lilly, C.M., Invited review: effects of heat and cold stress on mammalian gene expression. *Journal of Applied Physiology*, 92(4), pp. 1725-1742, 2002. DOI: <https://doi.org/10.1152/jappphysiol.01143.2001>.
- [10] Liu, Q., Frerck, M.J., Holman, H.A., Jorgensen, E.M. and Rabbitt, R.D., Exciting cell membranes with a blustering heat shock. *Biophysical Journal*, 106(8), pp. 1570-1577, 2014. DOI: <https://doi.org/10.1016/j.bpj.2014.03.008>.
- [11] de Meis, L., Uncoupled ATPase activity and heat production by the sarcoplasmic reticulum Ca²⁺-ATPase: regulation by ADP. *Journal of Biological Chemistry*, 276(27), pp. 25078-25087, 2001. DOI: <https://doi.org/10.1074/jbc.M103318200>.
- [12] Kjelstrup, S., Meis, L., Bedeaux, D. and Simon, J.-M., Is the Ca²⁺-ATPase from sarcoplasmic reticulum also a heat pump? *European Biophysics Journal*, 38(1), pp. 59-67, 2008. DOI: <https://doi.org/10.1007/s00249-008-0358-0>.
- [13] Ørtenblad, N., Macdonald, W.A. and Sahlin, K., Glycolysis in contracting rat skeletal muscle is controlled by factors related to energy state. *Biochemical Journal*, 420(2), pp. 161-168, 2009. DOI: <https://doi.org/10.1042/BJ20082135>.
- [14] González-Alonso, J., Quistorff, B., Krstrup, P., Bangsbo, J., Saltin, B. Heat production in human skeletal muscle at the onset of intense dynamic exercise. *The Journal of Physiology*, 524(2), pp. 603-615, 2000. DOI: <https://doi.org/10.1111/j.1469-7793.2000.00603.x>.
- [15] Yin, Y., Guo, Z., Chen, X. and Fan, Y., Studies on biomechanics of skeletal muscle based on the working mechanism of myosin motors: an overview. *Chinese Science Bulletin*, 57(35), pp. 4533-4544, 2012. DOI: <https://doi.org/10.1007/s11434-012-5438-y>.
- [16] Gautel, M. and Djinić-Carugo, K., The sarcomeric cytoskeleton: from molecules to motion. *Journal of Experimental Biology*, 219(2), pp. 135-145, 2016. DOI: <https://doi.org/10.1242/jeb.124941>.
- [17] Barclay, C.J., Woledge, R.C. and Curtin, N.A., Inferring crossbridge properties from skeletal muscle energetics. *Progress in Biophysics and Molecular Biology*, 102(1), pp. 53-71, 2010. DOI: <https://doi.org/10.1016/j.pbiomolbio.2009.10.003>.
- [18] Murrell, M., Oakes, P.W., Lenz, M. and Gardel, M.L., Forcing cells into shape: the mechanics of actomyosin contractility. *Nature Reviews Molecular Cell Biology*, 16(8), pp. 486-498, 2015. DOI: <https://doi.org/10.1038/nrm4012>.
- [19] Huxley, A.F., Mechanics and models of the myosin motor. *Philosophical Transactions of the Royal Society of London B: Biological Sciences*, 355(1396), pp. 433-440, 2000. DOI: <https://doi.org/10.1098/rstb.2000.0584>.
- [20] Morales, M.F., The search for a biological energy transducer. *American Zoologist*, 29(2), pp. 593-603, 1989.
- [21] Andraud, C., Lafait, J., Beghdadi, A. and Peiro, J., Entropy Applied to morphological analysis and modelisation of nanomaterial optical properties. *Journal de Physique III*, 7(3), pp. 549-557, 1997. DOI: <https://doi.org/10.1051/jp3:1997142>.
- [22] Andraud, C., Beghdadi, A. and Lafait, J., Entropic analysis of random morphologies. *Physica A: Statistical Mechanics and its Applications*, 207(1), pp. 208-212, 1994. DOI: [https://doi.org/10.1016/0378-4371\(94\)90374-3](https://doi.org/10.1016/0378-4371(94)90374-3).
- [23] Rodríguez-Iturbe, I., D'Odorico, P. and Rinaldo, A., Configuration entropy of fractal landscapes. *Geophysical Research Letters*, 25(7), pp. 1015-1018, 1998. DOI: <https://doi.org/10.1029/98GL00654>.
- [24] Mendoza, F., Valous, N.A., Sun, D.-W. and Allen, P., Characterization of fat-connective tissue size distribution in pre-sliced pork hams using multifractal analysis. *Meat Science*, 83(4), pp. 713-722, 2009. DOI: <https://doi.org/10.1016/j.meatsci.2009.08.009>.
- [25] Tarquis, A.M., McInnes, K.J., Key, J.R., Saa, A., García, M.R. and Díaz, M.C., Multiscaling analysis in a structured clay soil using 2D images. *Journal of Hydrology*, 322(1-4), pp. 236-246, 2006. DOI: <https://doi.org/10.1016/j.jhydrol.2005.03.005>.
- [26] Allen, D.G., Lamb, G.D. and Westerblad, H., Skeletal Muscle Fatigue: Cellular Mechanisms. *Physiological Reviews*, 88(1), pp. 287-332, 2008. DOI: <https://doi.org/10.1152/physrev.00015.2007>.
- [27] MacIntosh, B.R., Holash, R.J. and Renaud, J.-M., Skeletal muscle fatigue - regulation of excitation-contraction coupling to avoid metabolic catastrophe. *J Cell Sci*, 125(9), pp. 2105-2114, 2012. DOI: <https://doi.org/10.1242/jcs.093674>.
- [28] Feng, S. and Yang, L., Dynamical mechanisms of glycolytic oscillations in ventricular myocytes. in: 2010 International Workshop on Chaos-Fractal Theories and Applications, pp. 360-364, 2010.
- [29] Fu, Y., Zhang, G.-Q., Hao, X.-M., Wu, C.-H., Chai, Z. and Wang, S.-Q., Temperature dependence and thermodynamic properties of Ca²⁺ sparks in rat cardiomyocytes. *Biophysical Journal*, 89(4), pp. 2533-2541, 2005. DOI: <https://doi.org/10.1529/biophysj.105.067074>.
- [30] Bennett, A.F., Thermal dependence of muscle function. *American Journal of Physiology-Regulatory, Integrative and Comparative Physiology*, 247(2), pp. R217-R229, 1984. DOI: <https://doi.org/10.1152/ajpregu.1984.247.2.R217>.

D. Barragán, is an associate professor at the Escuela de Química, Facultad de Ciencias de the Universidad Nacional de Colombia Sede Medellín. Is BSc. in Chemist and Dr. in Chemistry, 2003. Research and teaching interests in non-equilibrium thermodynamics, nonlinear chemical dynamics, and physical chemistry.
ORCID: 0000-0002-7390-1104

P.A. Ochoa-Botache, received the BSc. Eng in Physical Engineering in 2013, and MSc. in Science - Chemistry in 2017. Since 2014 he has been professor in the Physics School, Universidad Nacional de Colombia, Medellín campus. His research interests include: simulation of biological systems from a thermodynamic perspective and education research in natural sciences. He is also currently coordinator of the Master in teaching of natural sciences and mathematics, Facultad de Ciencias, Universidad Nacional de Colombia – Medellín campus.
ORCID: 0000-0001-8565-7033